Putting Mechanics into Quantum Mechanics

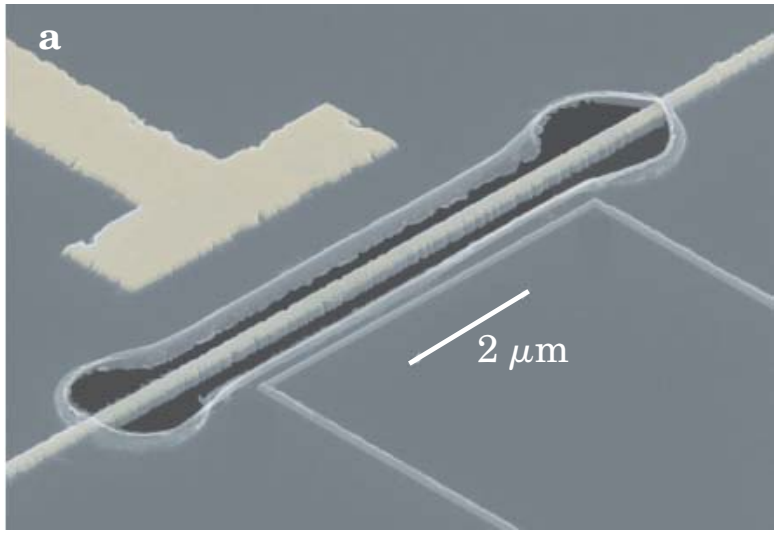

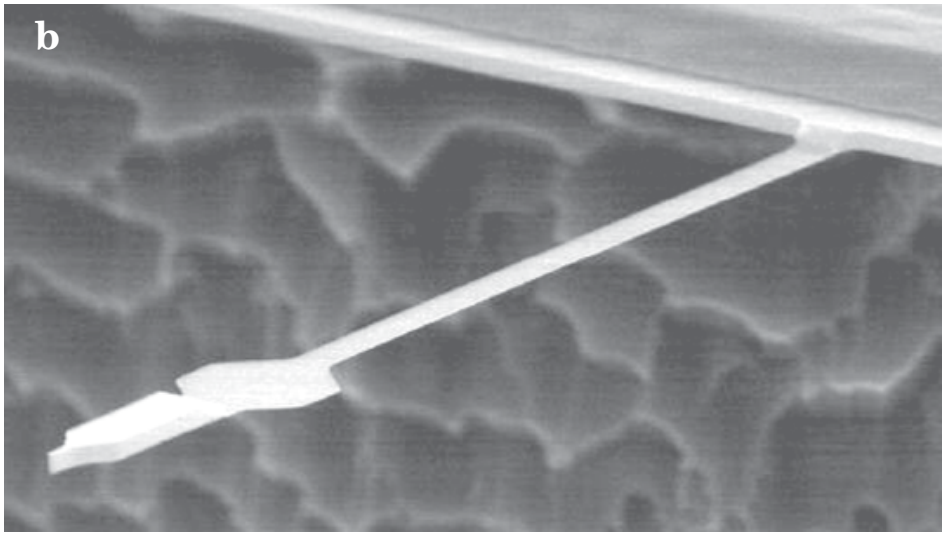

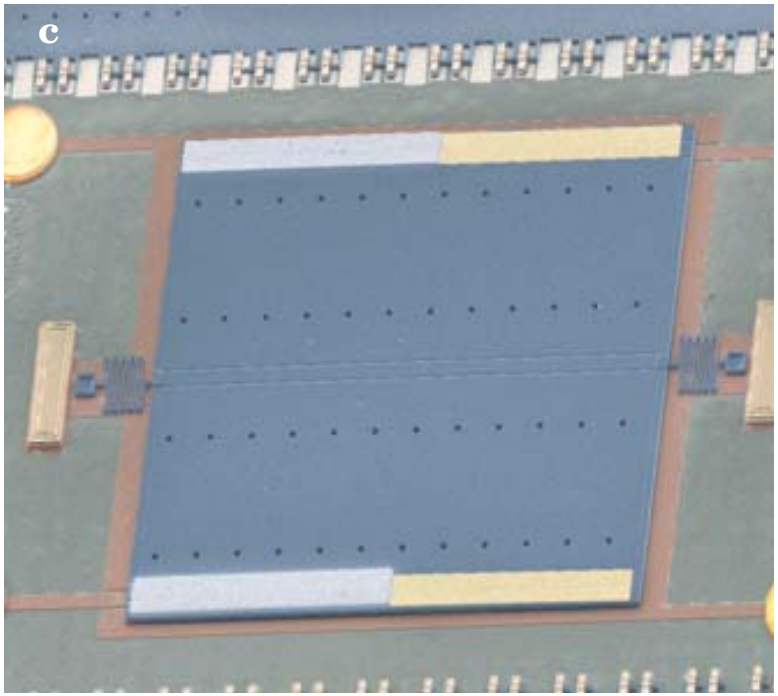

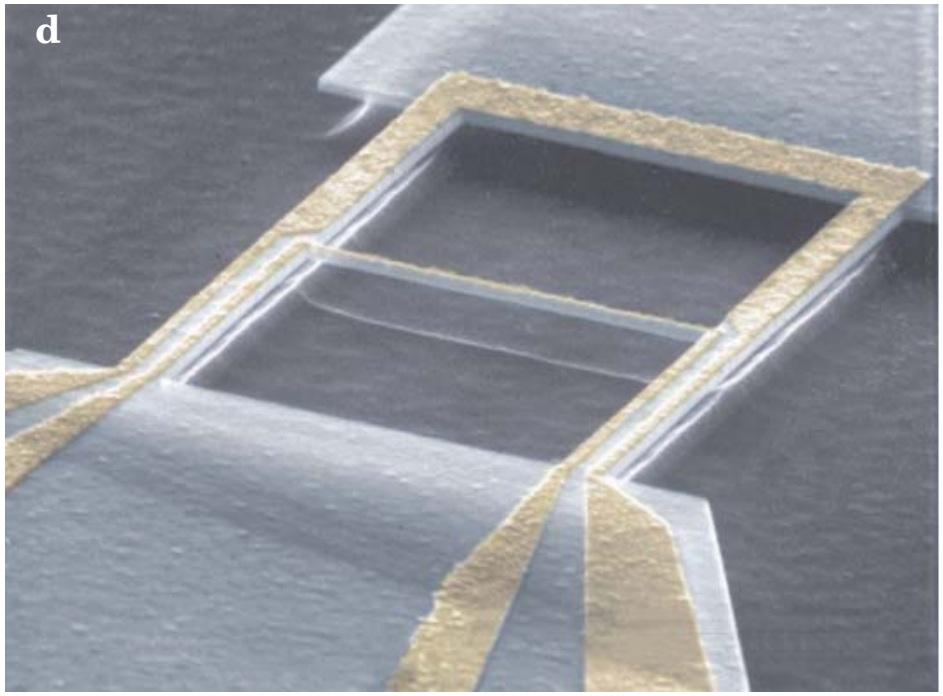

Putting Mechanics into Quantum Mechanics

Nanoelectromechanical structures are starting to approach the ultimate quantum mechanical limits for detecting and exciting motion at the nanoscale. Nonclassical states of a mechanical resonator are also on the horizon.

Keith C. Schwab and Michael L. Roukes

Today, micro- and nanoelectromechanical systems (MEMS and NEMS) are widely employed in ways similar to those early force detectors, yet with vastly greater force and mass sensitivity—now pushing into the realm of zeptonewtons (10^{-21} N) and zeptograms (10^{-21} g). These ultraminiature sensors also can provide spatial resolution at the atomic scale and vibrate at frequencies in the gigahertz range.[1] Among the breadth of applications that have become possible are measurements of forces between individual biomolecules,[2] forces arising from magnetic resonance of single spins,[3] and perturbations that arise from mass fluctuations involving single atoms and molecules.[4] The patterning of mechanical structures with nanometer-scale features is now commonplace; figure 1 and the cover display examples of current devices.

http://www.kschwabresearch.com/members/detail/12

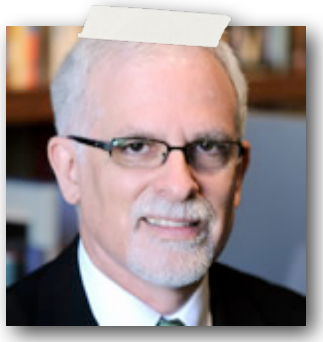

http://nano.caltech.edu/people/roukes-m.html

July 2005 Physics Today

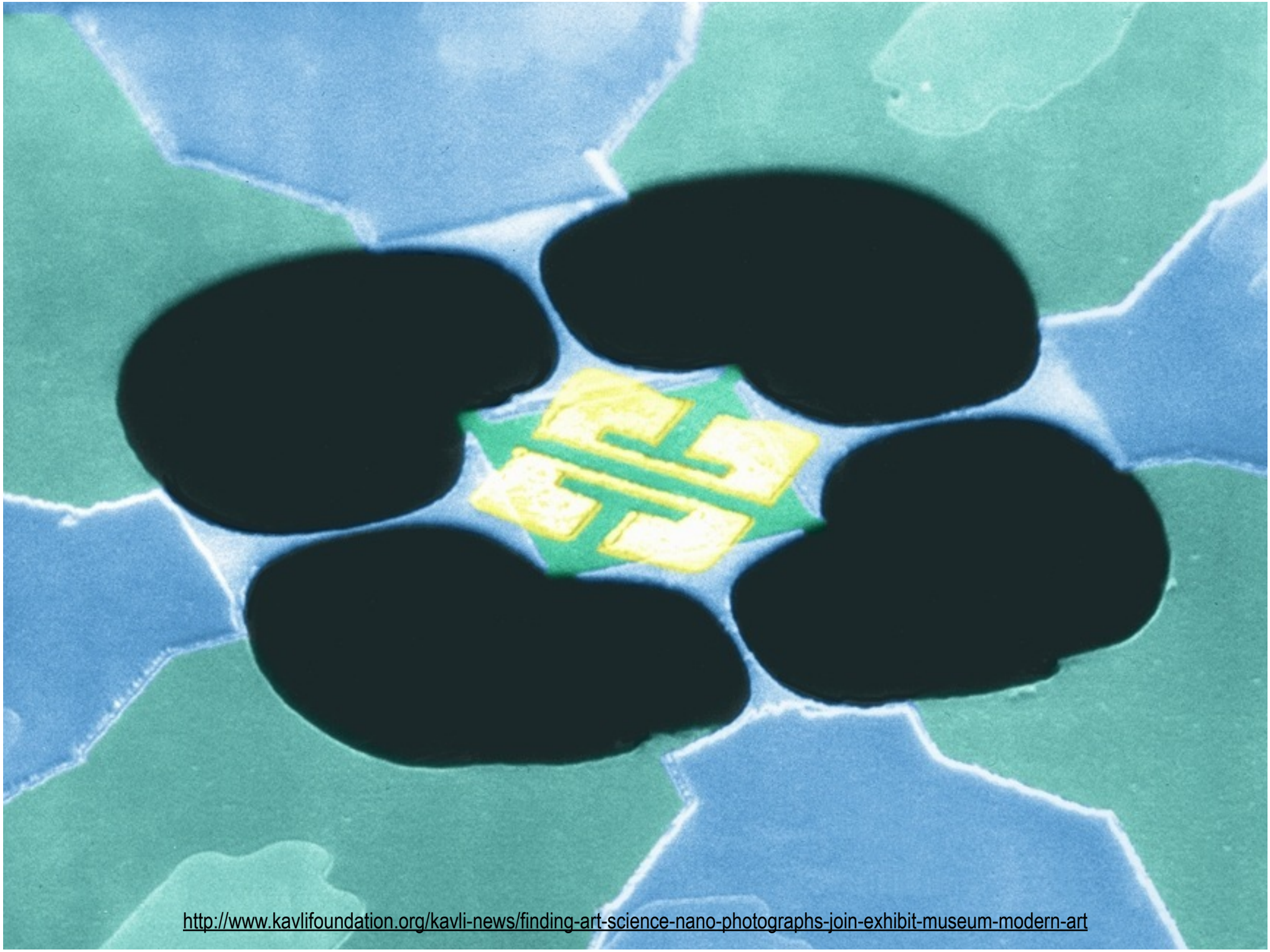

http://www.kavlifoundation.org/kavli-news/finding-art-science-nano-photographs-join-exhibit-museum-modern-art

What does it take to observe the quantum nature of an ordinary system?

REPORTS

Approaching the Quantum Limit of a Nanomechanical Resonator

M. D. LaHaye,[1,2] O. Buu,[1,2] B. Camarota,[1,2] K. C. Schwab[1]*

By coupling a single-electron transistor to a high–quality factor, 19.7-megahertz nanomechanical resonator, we demonstrate position detection approaching that set by the Heisenberg uncertainty principle limit. At millikelvin temperatures, position resolution a factor of 4.3 above the quantum limit is achieved and demonstrates the near-ideal performance of the single-electron transistor as a linear amplifier. We have observed the resonator's thermal motion at temperatures as low as 56 millikelvin, with quantum occupation factors of $N_{TH} = 58$. The implications of this experiment reach from the ultimate limits of force microscopy to qubit readout for quantum information devices.

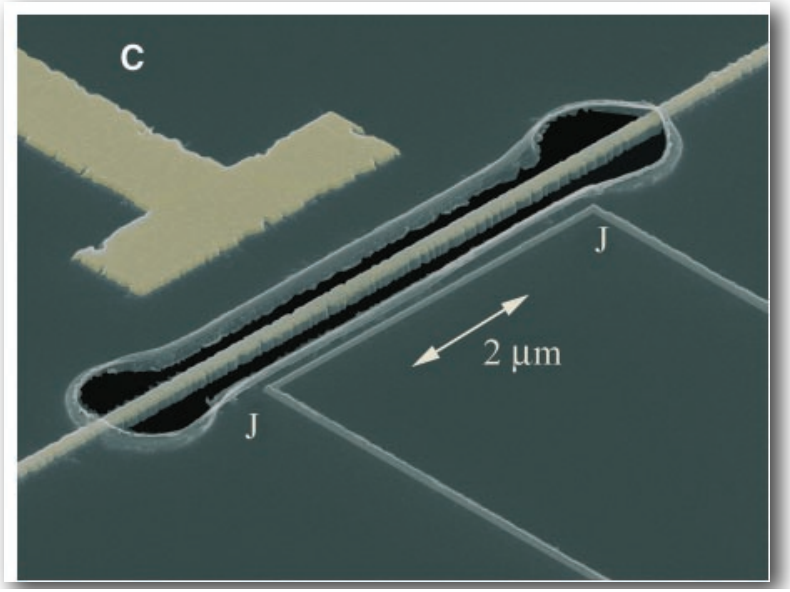

Outline

1. Mechanical resonator
2. Quantum modes and occupancy
3. SSET (superconducting single-electron transistor)
4. Measurements...

Outline

1. Mechanical resonator
2. Quantum modes and occupancy
3. SSET (superconducting single-electron transistor)
4. Measurements…

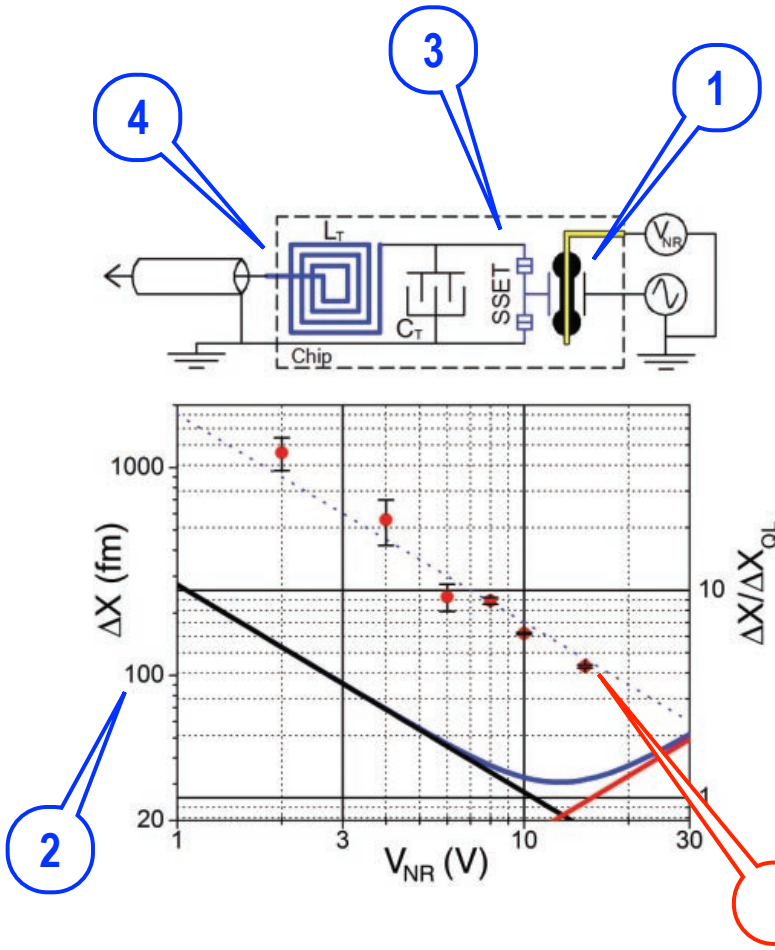

Fig. 1. (**Bottom**) The solid lines show the expected position resolution due to shot-noise (black), back-action noise (red), and the uncorrelated sum (blue) as a function of coupling voltage V_{NR}, assuming the device parameters realized in this experiment. The points are the observed sensitivity where the deviation from the blue curve is due to nonidealities in the RF-SSET readout circuit. The dashed line is the expected sensitivity calculated from the measured charge sensitivity. Error bars are on the quantity $\Delta X/\Delta X_{QL}$. (**Top**) The simplified schematic shows the RF-SSET capacitively coupled to a voltage-biased Au/SiN nanomechanical resonator with on-chip LC resonator formed by the square spiral, L_T, and an interdigitated capacitor, C_T.

100 fm = 10^{-13} m ~ size of 12 gold atoms

19.7 MHz Nanomechanical Resonator

(C) Details of the 19.7-MHz nanomechanical resonator (**200 nm wide, 8 µm long, coated with 20 nm of Au atop 100 nm SiN**), defined by the regions in black where the SiN has been etched through. The SSET island (5 µm long and 50 nm wide) is positioned 600 nm away from the resonator. Tunnel junctions, marked "J," are located at corners. A 70-nm-thick gold gate is positioned to the right of the resonator and is used both to drive the resonator and to control the bias point of the SSET.

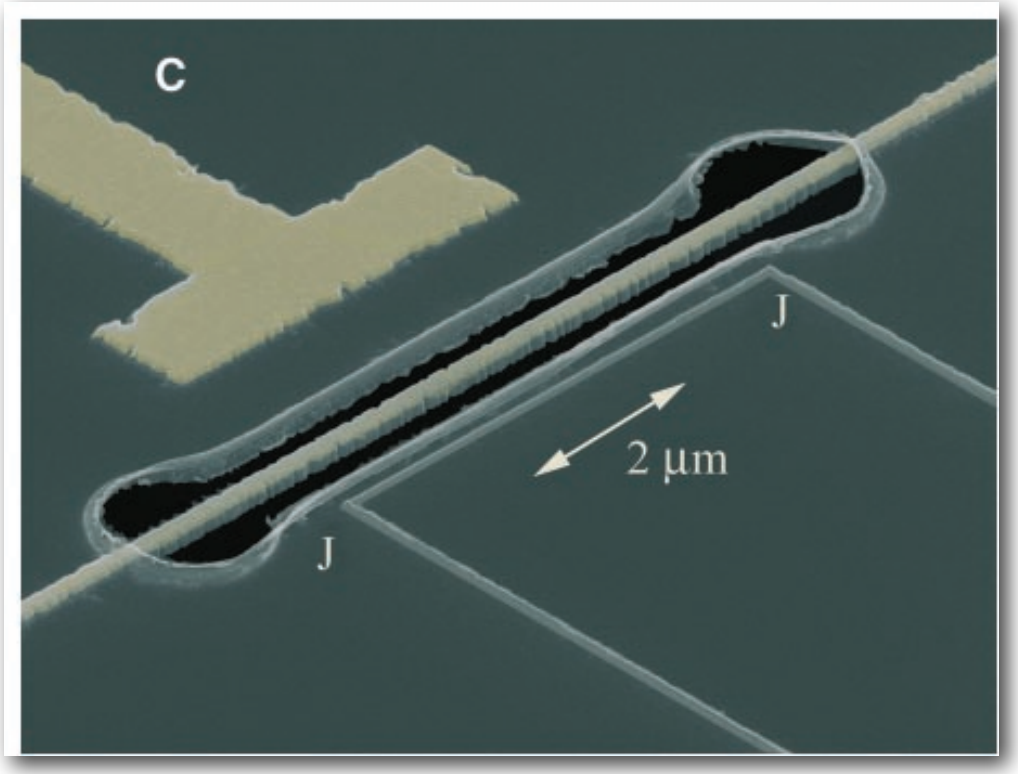

Vibrating Beam

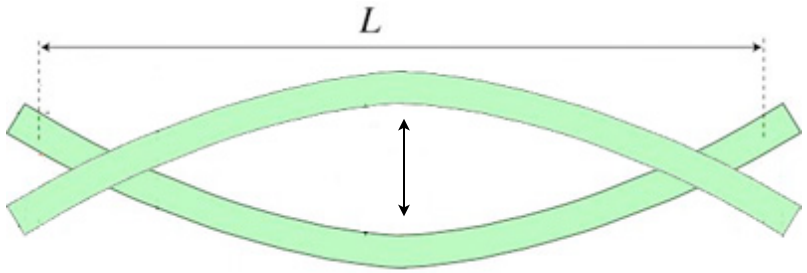

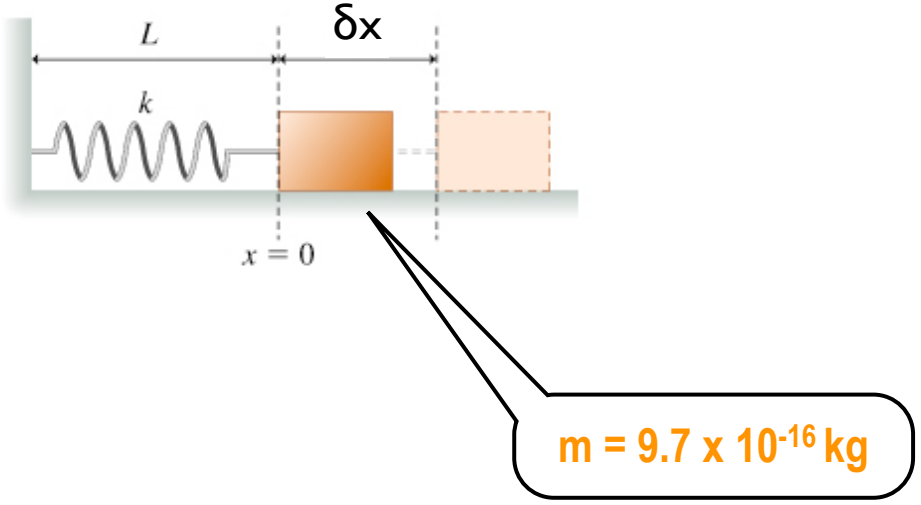

$2 \pi f = \sqrt{(k/m)}$

Quantum Harmonic Oscillator

$$i\hbar\frac{\partial\psi}{\partial t} = -\frac{\hbar^2}{2m}\frac{\partial^2\psi}{\partial x^2} + V(x)\psi$$

$$E_n\psi = -\frac{\hbar^2}{2m}\frac{\partial^2\psi_n}{\partial x^2} + V(x)\psi_n$$

$$\psi_n(x) \propto e^{-\beta^2 x^2/2} H_n(\beta x)$$

$$E_n = \hbar\omega\left(\frac{1}{2} + n\right) = \hbar\sqrt{k/m}\left(\frac{1}{2} + n\right)$$

Quanta of Oscillations

(Phonons)

T	n_i
1.4 mK	1
2.3 mK	2
47.7 mK	50

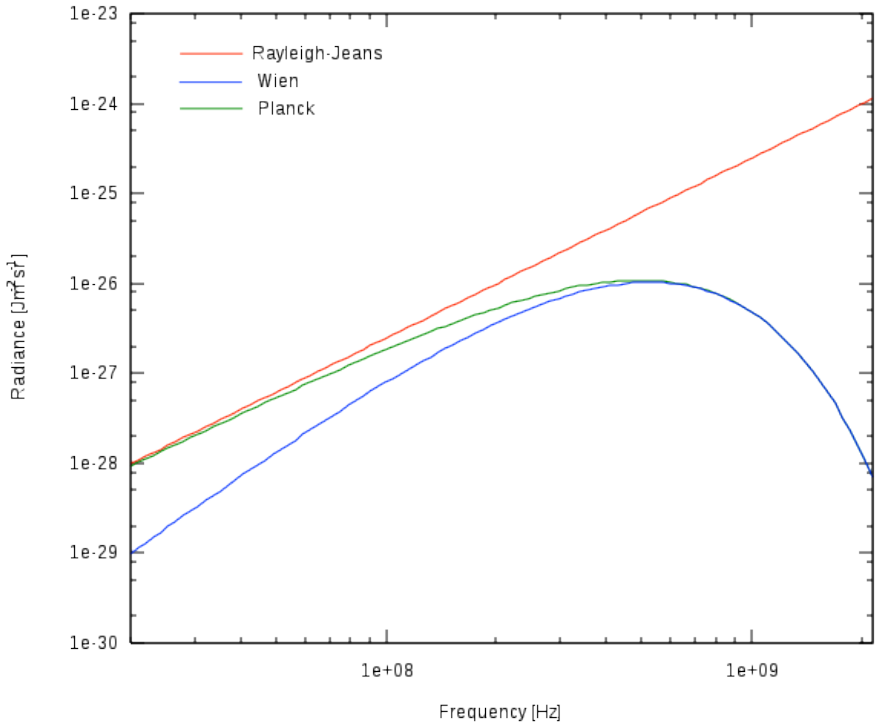

$$n_i = \frac{1}{\exp(\hbar\omega/kT) - 1} \rightarrow \frac{kT}{\hbar\omega} \text{ for } kT \gg \hbar\omega$$

Vibrating Beam

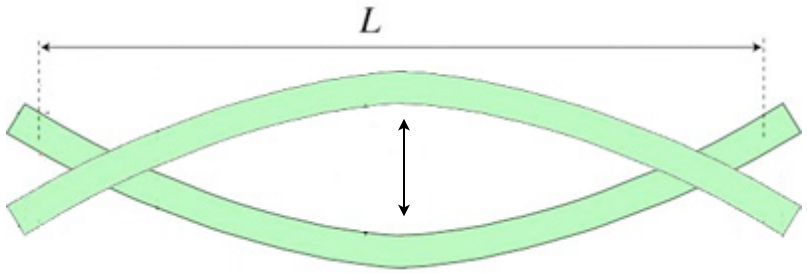

$$\rho \frac{\partial^2 \mathbf{u}}{\partial t^2} = \nabla \cdot \bar{\bar{\tau}}$$

$$\rho A \frac{\partial^2 \delta x}{\partial t^2} = \int dx dy \mu \frac{\partial^2 \delta x}{\partial z^2}$$

$$\bar{\bar{\tau}} = 2\mu \bar{\bar{\epsilon}}$$

$$\rho \frac{\partial^2 u_x}{\partial t^2} = \frac{\partial}{\partial z}\left(\mu \frac{\partial u_x}{\partial z}\right)$$

$$2\pi f = \frac{\pi}{2L}\sqrt{\frac{E}{\rho}\frac{I\pi^2}{AL^2}}$$

Young's & Shear Modulus (E, μ)

Material	Typical values for shear modulus (GPa)	Young's Modulus (GPa)	Mass Density (kg/m³)
Diamond[2]	478	1220	3,530
Steel[3]	79	200	~ 8,000
Copper[4]	45	117	8,960
Glass[3]	26	70	
Aluminium[3]	26	69	2,700
Rubber[5]	0.0006	~0.05	
Gold	27	79	19,300
Si_3N_4	~100	310	3,440

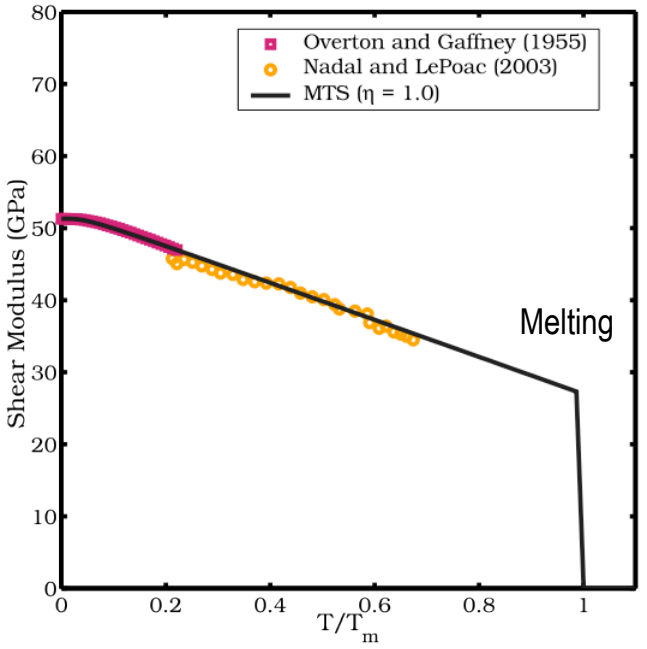

$$2\pi f = \frac{\pi}{2L}\sqrt{\frac{E}{\rho}\frac{I\pi^2}{AL^2}}$$

Measurement/Detection

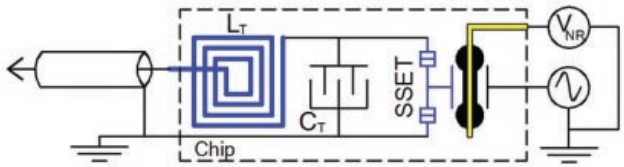

Fig. 1. (**Bottom**) The solid lines show the expected position resolution due to shot-noise (black), back-action noise (red), and the uncorrelated sum (blue) as a function of coupling voltage V_{NR}, assuming the device parameters realized in this experiment. The points are the observed sensitivity where the deviation from the blue curve is due to nonidealities in the RF-SSET readout circuit. The dashed line is the expected sensitivity calculated from the measured charge sensitivity. Error bars are on the quantity $\Delta X/\Delta X_{QL}$. (**Top**) The simplified schematic shows the RF-SSET capacitively coupled to a voltage-biased Au/SiN nanomechanical resonator with on-chip LC resonator formed by the square spiral, L_T, and an interdigitated capacitor, C_T.

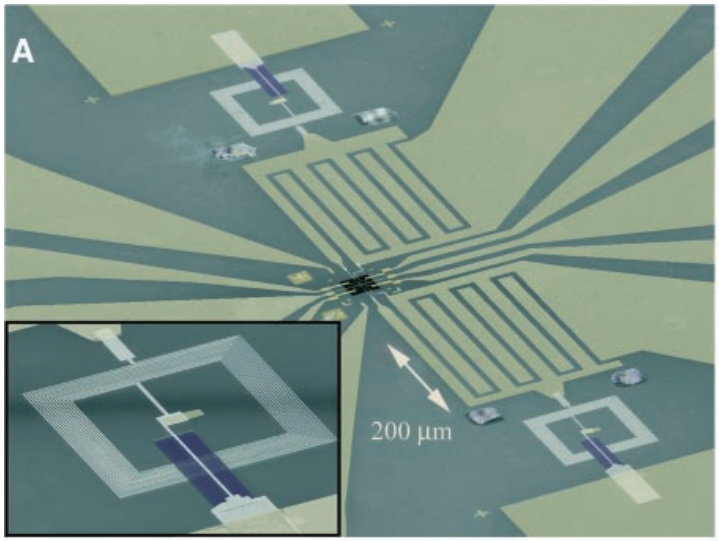

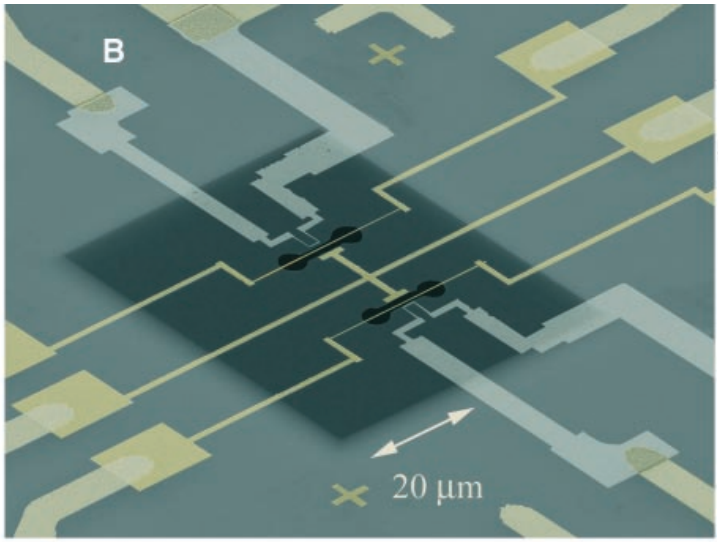

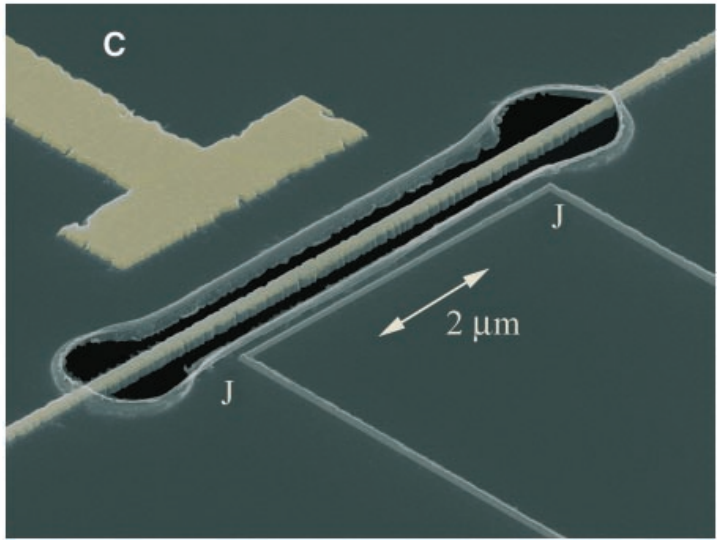

Fig. 2. Colorized scanning electron micrographs of the sample. (**A**) Metallizations (170 nm Al / 20 nm Ti / 20 nm Au) atop a [100] silicon wafer coated with 100 nm of SiN, which has been back-etched using KOH to form a 55-μm by 55-μm SiN membrane (shown as the black square in the center.) The Al/Ti/Au film is in contact with the silicon, which both provides electronic protection for the delicate device at room temperature and superconducts below 0.8 K. The inset on the left shows the 130-μm by 130-μm square coil used for the 1.35 GHz LC resonator. (**B**) SiN membrane (dark square), the Al leads to the SSET, and the Au leads to the nanomechanical resonator and electrostatic gates. (**C**) Details of the 19.7-MHz nanomechanical resonator (200 nm wide, 8 μm long, coated with 20 nm of Au atop 100 nm SiN), defined by the regions in black where the SiN has been etched through. The SSET island (5 μm long and 50 nm wide) is positioned 600 nm away from the resonator. Tunnel junctions, marked "J," are located at corners. A 70-nm-thick gold gate is positioned to the right of the resonator and is used both to drive the resonator and to control the bias point of the SSET.

SET

- The SET is based on the tunnel effect through a metal–insulator–metal junction.
- When two metallic electrodes are separated by an insulating barrier whose thickness is about 1 nm, electrons can traverse the insulator even though their energy is too low to overcome, in a classical motion, the large potential barrier of the insulating region. The tunnel effect manifests itself by a finite resistance R_T of the insulating barrier.
- For barriers with small tunneling, the charge Q transferred through the barrier becomes quantized. Q = Ne, where N is an integer.For N not to be subject to quantum fluctuations, the resistance of the junction must be large compared with the resistance quantum RT >> h/e^2 = 25.8 k Ohm.
- If the dimensions of the island are sufficiently small, the charging energy, $e^2/(2C_i)$, of one extra electron in the island will become larger than the energy of thermal fluctuations, kT.
- In practice, for devices fabricated by standard electron-beam lithography, C_i is of the order of a fF and the charging energy is of order 1 K. Temperatures must be below 300 mK to satisfy the above charging energy criterion.

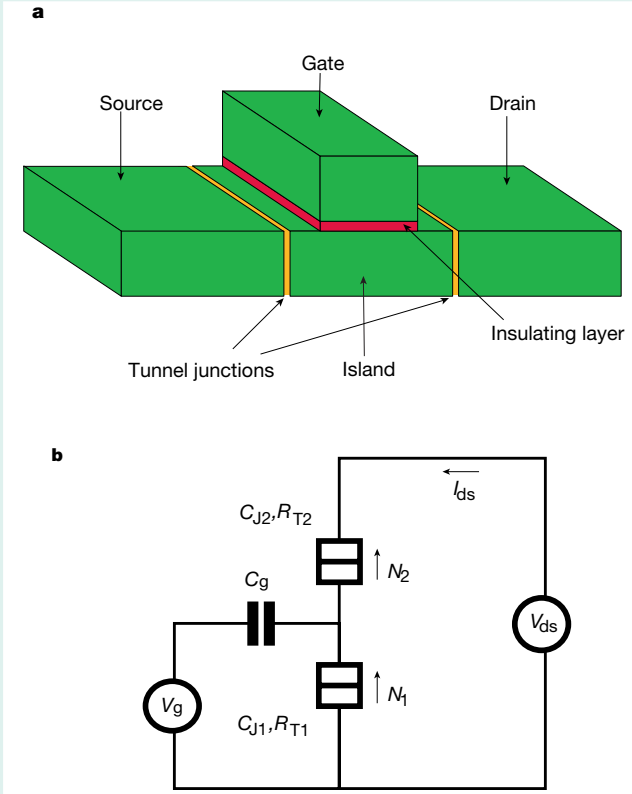

Figure 3 The single-electron tunnelling transistor (SET). **a**, Simplified three-dimensional structure of the SET. The channel of the FET is replaced here by a sandwich consisting of a nanoscale metal electrode (island), which is connected to the drain and the source by tunnel junctions. As in the FET, a gate electrode influences the island electrostatically. **b**, Circuit diagram of the SET. The square box symbol represents a tunnel junction, and integers N_1 and N_2 denote the numbers of electrons having tunnelled through the two junctions. Each junction is characterized by its capacitance and its tunnel resistance.

Noise Power at Resonance

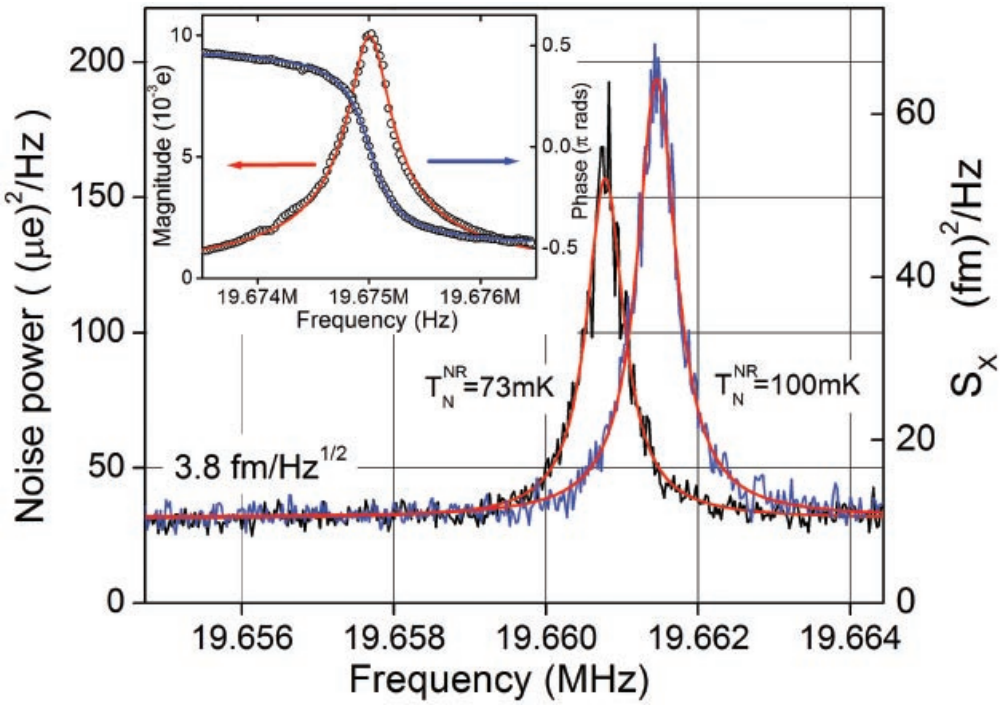

Fig. 3. Charge noise power around the mechanical resonance with V_{NR} = 15 V. Right peak is taken at 100 mK and is fit with a Lorentzian, shown as a red line. This noise power is used to scale the left peak taken with the refrigerator at 35 mK and corresponds to a resonator noise temperature of T_N^{NR} = 73 mK. This then scales the white-noise floor, which corresponds to a system-noise temperature of T_N^{SSET} = 16 mK = 18 T_{QL}. Using the equipartition relation, the displacement resolution is 3.8 fm/$\sqrt{\text{Hz}}$. The inset shows the driven response, approximately 800 pm on resonance, with the data as circles and a Lorentzian fit as the solid lines. All SSET measurements are taken with the SSET biased near the double Josephson quasiparticle resonance peak.

Occupation

Fig. 4. The integrated charge noise power, PNR, scaled by V_{NR}, versus refrigerator temperature for different V_{NR}. Right axis shows the quantum occupation factor, N_{TH}. Above 100 mK, we find excellent agreement with classical equipartition of energy, $P_{NR} \propto T$, shown as the solid line through the origin. Below 100 mK, we observe a deviation from this relationship, indicating a difficulty in thermalizing the nanomechanical mode. The arrow indicates the lowest observed noise temperature, $T_N^{NR} = 56$ mK and $N_{TH} = 58$. The upper plot shows both the quality factor, Q, and the resonant frequency shift, $\Delta F = F(T) - F(35\ mK)$, versus temperature, which are extracted by fitting the thermal noise peaks at $V_{NR} = 6$ V.

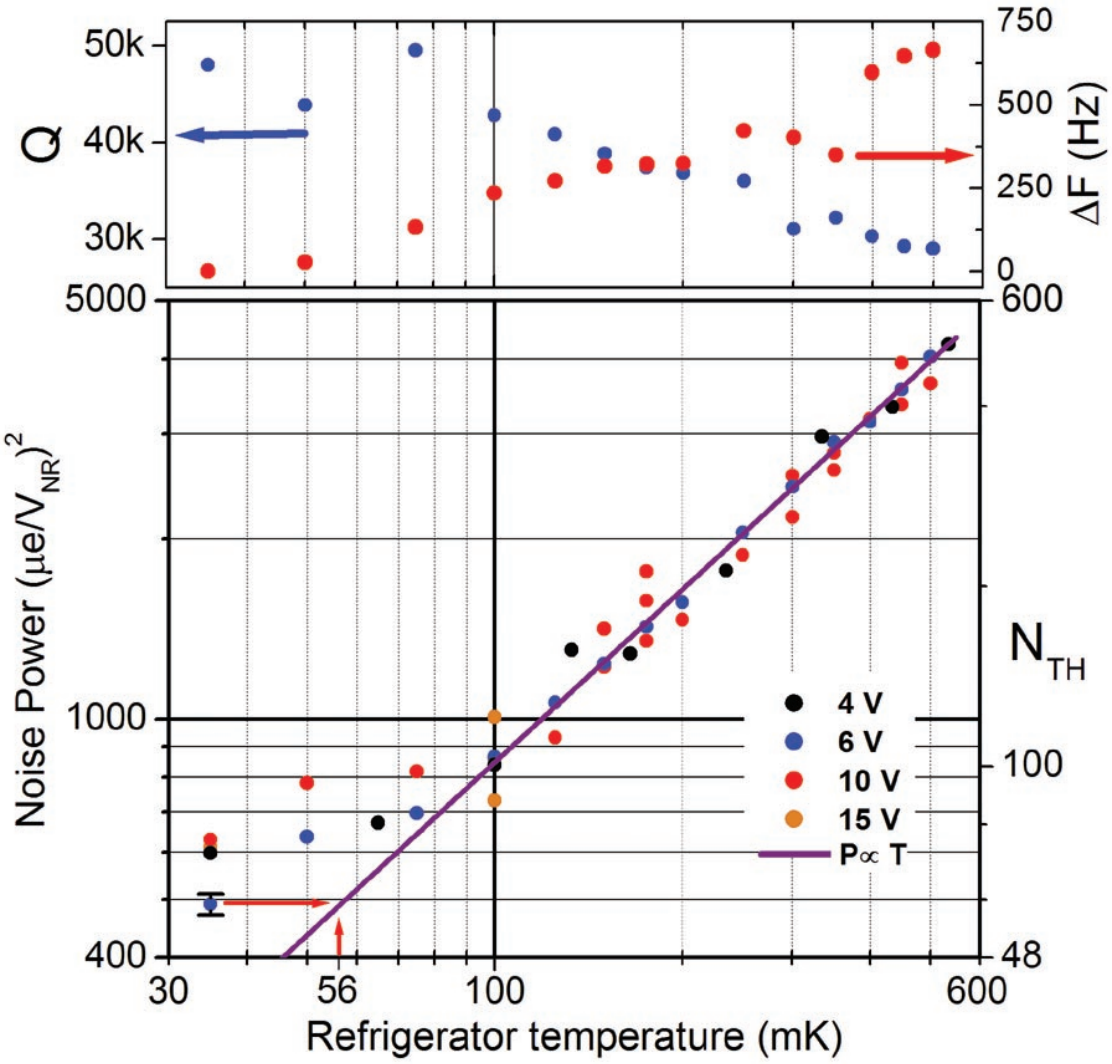

Next Week: LIGO

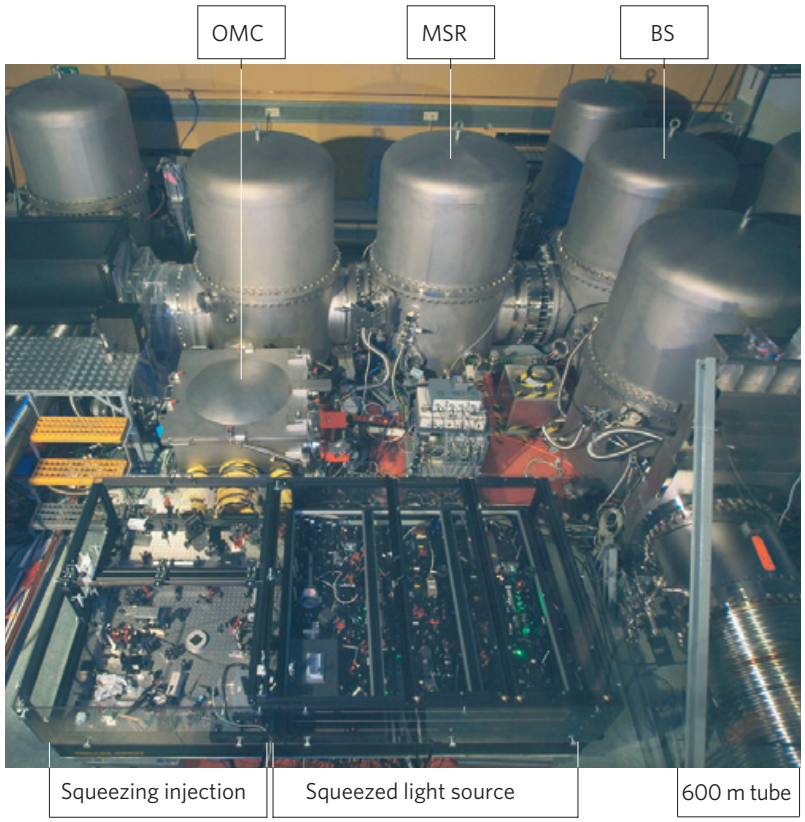

Figure 2 | View into the GEO 600 central building. In the front, the squeezing bench containing the squeezed-light source and the squeezing injection path is shown. The optical table is surrounded by several vacuum chambers containing suspended interferometer optics.

NATURE PHYSICS | VOL 7 | DECEMBER 2011

Although our measurements at 20 MHz are essentially immune to nonintrinsic noise, which is ubiquitous at acoustic frequencies, it is interesting to compare our approach to the quantum limit with the current sensitivity of ultrasensitive gravitational wave detectors. The 4-km Laser Interferometer Gravitational-Wave Observatory (LIGO) interferometric detector has achieved $\Delta x = 1000 \cdot \Delta x_{QL}$ (*22*) at 100 Hz. A tabletop optical interferometer has achieved $\Delta x = 23 \cdot \Delta x_{QL}$ on the 2 MHz vibrational modes of a 100-g silica mirror at room temperature (*23*). The best performance on the readout of displacement transducers for cryogenic, acoustic gravitational wave detectors at 1 KHz is $\Delta x = 167 \cdot \Delta x_{QL}$ (*24*), with thermal occupation $N_{TH} \sim 10^9$.